A thermal fluid-dynamic transient analysis of the EADF down-comer channel

C. Aragonese, S. Buono, G. Fotia, L. Maciocco, V. Moreau, L. Sorrentino

Cagliari, December 5, 2000

Abstract

In this work a numerical simulation of the downcomer channel of the Energy Amplifier Demonstration Facility (EADF) [1, 2] is presented. The simulation is fully three-dimensional (3D) and is focused on a transient analysis. All relevant heat transfer phenomena are taken into account.

Starting from the nominal power configuration, we have simulated the response of the system to a power shutdown of the core for aperiod of $60\ s$. The core shutdown is simulated imposing a linear variation of the inlet flow temperature from 400^oC to 305^oC in $10\ s$. The simulation shows the evolution of the thermal stratification outside the IHX and the evolution of the IHX operation.

1 Introduction

The Intermediate Heat eXchangers (IHXs) of the EADF reference configuration are immersed in the lead-bismuth eutectic of the down-comer channel. Because there is no physical barrier separating the hot and cold collectors, the percentage of the coolant flowrate that flows inside the IHX depends on the weight difference between the cooled fluid inside the IHX and the hot fluid beside it and, precisely, it is determined by the equilibrium between the above weight difference (driving force) and the pressure loss through the IHX.

Besides the IHX performance, an important aspect of the thermal-hydraulic design of the downcomer subsystem is that the thermal stresses have to be kept as low as possible, avoiding strong thermal gradients in the critical parts of the structure. The position and intensity of such gradients is evidentiated by the numerical simulation.

A one-dimensional simulation of the overall circuit can be found in [3], and a one-dimensional simulation of the downcomer channel can be found in [4]. Other studies have been done on other specific parts of the system [5, 6]. Here we are interested in the flow circulation of the primary coolant in the downcomer of the primary circuit. A first analysis on a simplified 3D geometry has already been done in [7]. A complete steady-state 3D parametric analysis has already been done in [8] and serves as a starting point for the present paper which focuses on the thermal fluid-dynamic analysis for a transient flow configuration characteristic of the transition from nominal to residual power operation.

2 Geometric description

The global geometric description of the EADF downcomer channel is shown in figure 1.

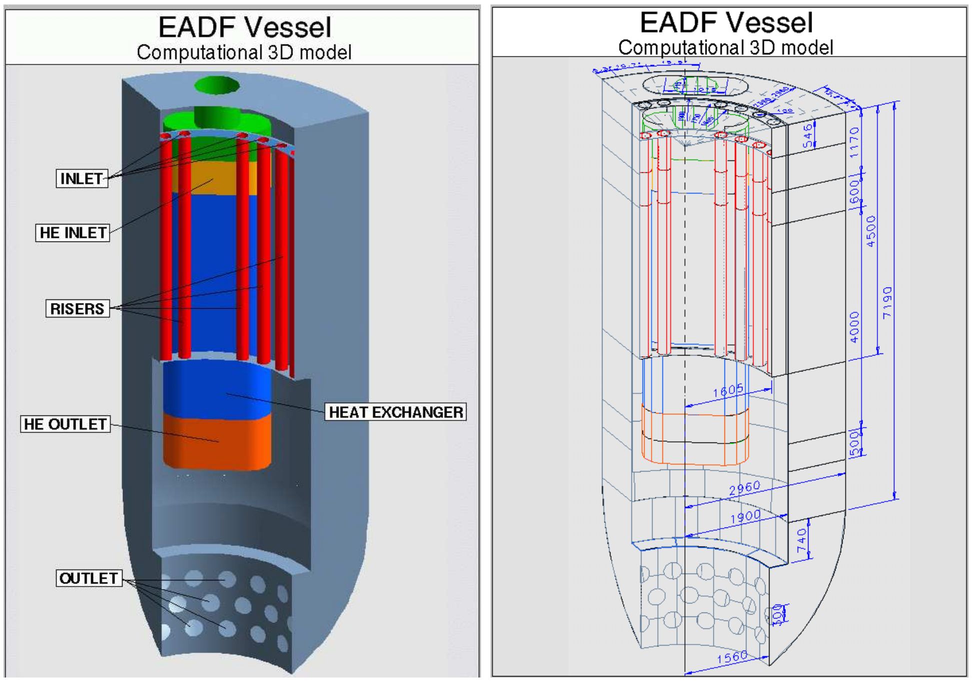

Figure 1: One quarter of the EADF downcomer channel. Distances are in millimeters.

Only a quarter of the full domain is simulated for symmetry reasons [8]. The Pb-Bi eutectic enters the domain rising inside the vertical red pipes and leaves the domain at the bottom part through a drilled shell to turn back to the core. The yellow and blue parts represent the IHX. The yellow part is unshielded and the flow enters at this level. The blue part is shielded and the orange part is just the shell guiding the flow vertically under the IHX (skirt). The green part is the secondary coolant feeding tube.The upper shell of the domain simulates the free surface.

3 General Parameters

3.1 Global Parameters

The global parameters of the primary circuit are reported below. The values of the extensive parameters are reported both for the whole vessel and for the quarter of the vessel effectively simulated.

Coolant: Lead-Bismuth Eutectic

Nominal power: $P_w = 4 \times 20.75 = 83\ MW$

Mass flow rate: $\dot{M} = 4 \times 1449 = 5.8 \cdot 10^3\ kg\, s^{-1}$

Volume flow rate: $\Phi_{inlet} = 4 \times 0.142 = 0.57\ m^3\, s^{-1}$

Reference temperature $T_{ref} = 673\ K = 400\ ^oC$

Inlet temperature $T(t) = Max(400 - 9.5 \times t, 305)$ **with** $T(t)$ **in** ^oC.

Volume of coolant: $Vol_c = 4 \times 37.5 = 150\ m^3$

3.2 Coolant properties

The values reported below are taken from [9]. Reference values corresponding to the reference temperature are also reported.

Density: $\rho = 10186\ kg\, m^{-3}$ **at** $T_{in} = 400\ ^oC$

$$\rho = \begin{cases} 11112 - 1.375T & \text{(T in } K) \\ 10737 - 1.375T & \text{(T in } ^oC) \end{cases} \tag{1}$$

Laminar viscosity: $\mu = 1.50 \cdot 10^{-3}\ kg\, m^{-1}\, s^{-1}$ **at** $T_{in} = 400\ ^oC$

$$\mu = \begin{cases} 4.71 \cdot 10^{-9}T^2 - 8.92 \cdot 10^{-6}T + 5.37 \cdot 10^{-3} & \text{(T in } K) \\ 4.63 \cdot 10^{-9}T^2 - 6.26 \cdot 10^{-6}T + 3.26 \cdot 10^{-3} & \text{(T in } ^oC) \end{cases} \tag{2}$$

Specific heat: $Cp = 146.5\ J\, kg^{-1}\, K^{-1}$

Thermal conductivity: $k = 12.2\ W\,m^{-1}\,K^{-1}$ at $T_{in} = 400\ ^oC$

$$k = \begin{cases} 3.90 + 0.0123T & \text{(T in } K) \\ 7.26 + 0.0123T & \text{(T in } ^oC) \end{cases} \tag{3}$$

Melting point: $T_M = 398\ K = 125\ ^oC$

Boiling point: $T_B = 1912\ K = 1639\ ^oC$ at $101\,325\ Pa$.

4 IHX main geometrical characteristics

The IHXs are of the bayonet type [2] and are immersed in the primary coolant (Pb-Bi) without any solid structure separating the hot and cold collectors in the region around the IHXs.

The IHX is enclosed in a 2cm steel shell, except for the upper 60 cm which serve as inlet region. The skirt goes 90cm deeper than the tubes to enhance the pumping effect. The characteristics relevant for the numerical simulation are given below:

Volume: $Vol_{ihx} = 5.36\ m^3$

Superficial area: $A = 1.16\ m^2$

Height: $H = 4.6\ m$

Heat exchange surface: $S_{ihx} = 425\ m^2$

Number of tubes: $N_{tu} = 1364$

Tubes thickness: $\delta r = 1.2446 \cdot 10^{-3}\ m$

Tubes external radius: $R_{tu} = 11.112\ mm$

Perimeter: $Per = 4.34\ m$

Porosity: $Por = \frac{1}{A} \cdot (A - N_{tu}\pi R_{tu}^2) = 0.544$

Hydraulic diameter: $D = \frac{4A \cdot Por}{Per + N_{tu}.2\pi R_{tu}} = 0.0249\ m$

The following parameters are defined:

Reynolds number [1]: $Re_{ihx} = \frac{\rho \bar{v}_{ihx} \cdot D}{\mu}$

[1]where μ is the eutectic viscosity, ρ its density and $\bar{v}_{ihx}$ is the mean fluid velocity in the IHX

Pressure drop coefficient [2]: $f = 0.079 Re_{ihx}^{-0.25}$

Distributed pressure drop [3]: $\Delta P_r = \frac{2\rho f H \bar{v}_{ihx}^2}{D}$

5 Numerical implementation

5.1 Symmetry

We have simulated only one quarter of the domain, which allows a correct description of the inlet flow distribution. This approximation is expected to be irrelevant while the gain in computational resources is critical. A symmetry boundary condition has been imposed on the cutting sections.

5.2 Free Surface

The free surface at the top of the coolant is not simulated. We just put a rigid horizontal wall in correspondence of the mean surface level that the fluid is expected to reach under nominal operating condition. The simulation of the free surface is quite expensive from the computational point of view and its reliability is not clearly established. Moreover, the inlet flow should be a bubbly flow, with the bubbles escaping through the free surface. The combined effect on the flow of the presence of the bubbles, the free surface and their interaction is not known and should be the object of future studies. Anyway, the effect of the presence of the free surface is expected to be localized to the upper part of the domain and have a minimum influence on the thermal-hydraulic field in the rest of the domain.

5.3 Inlet

5.3.1 Geometrical considerations

The inlet consists of 24 holes corresponding to the outlet of the 24 rising pipes of $r_{pipe} = 0.1\ m$ internal radius for a total inlet area of $A_{inlet} = 24\pi r_{pipe}^2 = 4 \times 0.1885 = 0.7540\ m^2$. There are six inlet pipes in the computational domain. Previous simulations [7] have shown that the geometrical description of the pipes should not be excessively rough. A special effort has been made to describe all pipes to a relative high level of accuracy. The pipes section is approximated with an octagon inscribed in the real circular perimeter. The pipes interior is not simulated but their upper (octagonal) extremity is decomposed in 24 cells for the inflow description.

[2] Based on a relative roughness close to 0.0008 and a Reynolds number close to 40000, according to [10].

[3] Darcy's formula

5.3.2 Mass flow rate

The inlet mass flow rate is calculated in order to satisfy the relation

$$\dot{M}C_p\Delta T = P_w \tag{4}$$

with a small correction to take into account the global heat transfer balance through the walls. The inlet temperature is $T_{inlet}(0) = 400\ ^oC$ at the beginning of the simulation and decreases linearly to $T_{inlet}(10) = 305\ ^oC$ in $10\ s$. The final value is kept constant for the remaining $50\ s$. Because of the temperature variation, we cannot preserve both the mass flow rate and the volume flow rate. For practical reasons, we preserve the volume flow rate.

Taking into account the discrepancy between the surface of a disk and the surface of the inscribed octagon, the effective numerical inlet surface and inlet fluid velocity are:

$$A_{inlet} = 24 \times 2\sqrt{2}r_{pipe}^2 = 0.679\ m^2, \tag{5}$$

$$v_{inlet} = \Phi_{inlet}/A_{inlet} = 0.838\ m\,s^{-1}. \tag{6}$$

5.3.3 Turbulent parameters

The inlet turbulent intensity $\mathcal{I}_{inlet}$ and the turbulent length l_{inlet} must be specified when applying the $k - \varepsilon$ turbulence model. We assign $l_{inlet} = 0.2\ m$, equal to the diameter of the inlet tubes, and $\mathcal{I}_{inlet} = 0.01$. Both values have no real justification, but it has little relevance for this flow configuration.

5.4 Outlet

In [7], we simulated only the cylindrical part of the vessel down to the level -6920 mm. Unfortunately the simulation result gave inflow through the outlet. So we added the bottom region, simulating the outlet holes as one single centered rectangular big outlet of the same total area to simplify the mesh modelling.

5.5 Heat exchanger

5.5.1 Pressure losses

A detailed simulation of the IHX would have prohibitive computational costs. Therefore, it is simulated as a porous media. The Darcy's formula is used to calculate a local momentum source equivalent to the theoretical pressure loss. The local implementation of the Darcy's formula in term of the global hydraulic diameter is acceptable because the cell hydraulic diameter is nearly equal to the global hydraulic diameter. The resulting vertical momentum source term $\dot{S}_w$ is given by

$$\dot{S}_w = -C_1 \cdot |w_s|^{0.75} \cdot w_s \tag{7}$$

with

$$C_1 = -\frac{0.079 \cdot 2 \cdot \mu^{0.25} \cdot \rho^{0.75}}{D^{1.25} \cdot Por^{1.75}} \quad (8)$$

where w_s is the superficial vertical velocity, namely $w_s = Por \cdot w$ where w is the real vertical velocity. Note that this expression is valid only for a given range of Reynolds number, and should scale like w_s at very low Re_{ihx} and like w_s^2 for very high Re_{ihx}.

The value of C_1 is calculated using the values of the the physical parameters at 350^oC:

$$C_1 = 1.0024 \cdot 10^4 \, kg \, m^{-3.75} \, s^{-0.25}. \quad (9)$$

The treatment of the non-linearity in w_s can be done by mean of a user-subroutine or using a direct feature of the software allowing for a linear plus quadratic approximation of $\dot{S}$:

$$\dot{S}_w = -C_2 \cdot w_s - C_3 \cdot w_s^2. \quad (10)$$

Note that, according to [11] (chapter 8), C_2 should be strictly positive in presence of a stagnation point, as it is the case on top of the IHX, for numerical stability reasons. For the same reasons, a direct implementation through user-subroutine should introduce a cut-off value under which $\dot{S}_w$ is linear in w_s.

We cannot take the simpliest choice of taking $\dot{S}_w$ linear in w_s as we have done in [8] because we expect strong variations of the flow rate through the heat exchanger. We also want the flow rates close to the nominal flow rate, corresponding to a mean superficial velocity of $V_{s0} = 0.1224 \, m \, s^{-1}$, to be correctly simulated. For these reasons we take the curve given by equation 10 which is tangent in V_{s0} to the curve given by equation 7 [4], namely

$$\dot{S}_w = -C_1.[\frac{3}{4}|V_{s0}|^{-0.25} \cdot |w_s| + \frac{1}{4}|V_{s0}|^{0.75}] \cdot w_s. \quad (11)$$

By the way, this value is only indicative, being the length and arrangement of the IHX tubes subject to variations.

The IHX inlet is lateral and 60 cm high, so it is not trivial to define the IHX length if one wants to calculate, say, the pressure drop through the IHX using a 1D correlation. Anyway, we need to define in a consistant way the global friction pressure drop ΔP_f and the global buoyancy pressure gain ΔP_b for the IHX.

Our approach is based on the calculation of global work of friction and buoyancy forces scaled by the volume flow rates.

[4] The discrepancy between this curve and a best-fit curve on $[0; 1.7V_{s0}]$ is less than 2%.

We call $\dot{W}_f$ the work of the friction force, $\vec{\dot{S}} = (\dot{S}_u, \dot{S}_v, \dot{S}_w)^T$, per unit time:

$$\dot{W}_f = \int_{IHX} \vec{\dot{S}} \cdot \vec{v_s}. \tag{12}$$

We call

$$\vec{F_b} = -\beta(T - T_{ref}) \cdot \vec{g} \tag{13}$$

the buoyancy force, where T_{ref} is the reference temperature ($T_{ref} = 400\ ^oC$).

We call $\dot{W}_{b,in}$ and $\dot{W}_{b,out}$ the work of the buoyancy force per unit time inside the IHX and outside the IHX:

$$\dot{W}_{b,in} = \int_{IHX} \vec{F_b} \cdot \vec{v_s} \tag{14}$$

$$\dot{W}_{b,out} = \int_{IHX\,outside} \vec{F_b} \cdot \vec{v_s}. \tag{15}$$

We define the friction pressure drop ΔP_f to be:

$$\Delta P_f = \frac{\rho \dot{W}_f}{\dot{M}_{ihx}} \tag{16}$$

and we define the buoyancy pressure gain ΔP_b to be:

$$\Delta P_b = \frac{\rho \dot{W}_{b,in}}{\dot{M}_{ihx}} - \frac{\rho \dot{W}_{b,out}}{\dot{M} - \dot{M}_{ihx}}. \tag{17}$$

When the flow outside the IHX vanishes the second term of the right-hand-side in the above equation becomes undefined and we replace equation 17 with the following:

$$\vec{\tilde{F}_b} = -\beta(T - \bar{T}_{out}(z)) \cdot \vec{g} \tag{18}$$

$$\Delta P_b = \frac{\rho}{\dot{M}_{ihx}} \int_{IHX} \vec{\tilde{F}_b} \cdot \vec{v_s} \tag{19}$$

where $\bar{T}_{out}(z)$ is the average temperature outside the IHX over the plane of level z.

The quantities ΔP_b and ΔP_f can be calculated in post-processing and will be given in the results section.

The friction factor ξ used in reference [4] (pressure loss $\Delta P_f = \xi \cdot \frac{w^2}{2} \cdot \rho$) is obtained from ΔP_f by the formula:

$$\xi = \frac{2\rho \cdot Por^2 \cdot A^2}{\dot{M}_{ihx}^2} \cdot \Delta P_f \tag{20}$$

having used $w = \frac{\dot{M}_{ihx}}{\rho \cdot A}$, where $\dot{M}_{ihx}$ is the actual mass flow rate through the IHX. When it is equal to the total mass flow rate $\dot{M}$, then we have, for a porosity of 0.5:

$$\xi = 3.28 \cdot 10^{-3} \cdot \Delta P_f. \tag{21}$$

5.5.2 Enthalpy equation

Both the primary and the secondary coolant are simulated. The IHX region is modelled as a group of three porous media occupying the same physical space. The first one is dedicated to the primary coolant and has already been described. The two others are dedicated to the secondary coolant, one for the descending flow and one for the ascending flow. The heat transfer is simulated by adding a source term $\dot{H}_{he}$ in the enthalpy equation which is proportional to the temperature difference at the same position between pairs of cells in the porous media. The primary coolant and the descending secondary coolant exchange heat with the ascending flow region. The heat transfer is also proportional to the density of exchange surface (S_{he}/Vol_{he}) and to the IHX global heat transfer coefficient. The overall heat exchange coefficients are assumed constant and their value, calculated in [4, 12], are:

$$G_p = 1.1586 \cdot 10^5\ W\,K^{-1}\,m^{-3} \quad \text{primary-secondary coolant} \tag{22}$$

$$G_s = 0.5228 \cdot 10^5\ W\,K^{-1}\,m^{-3} \quad \text{rising-downcoming secondary coolant.} \tag{23}$$

5.6 Heat transfer accross solid walls

Apart from the primary-secondary coolant heat transfer, many other heat exchanges have been taken into account accross solid walls in the computational domain. On a case-by-case basis, we have used specific features of the code. In the following, we give a description of the heat transfer implementation. The walls location is shown on a radial profile of the downcomer channel in figure 2. The capital letters given below refer to the capital letters in this figure.

- **Heat Flux**: the EADF can release heat through a safety device called RVACS, which is external to the vessel and is based on the natural convection of external (ambient) air. The heat flux (ψ) depends on the Vessel outer wall temperature (T_w, expressed in ^oC) according to the following law[13]:

  $$\psi \;=\; -158. + 1.57 \cdot T_w - 1.52 \cdot 10^{-2} \cdot T_w^2 \text{ in } W\ m^{-2}. \tag{24}$$

  This law is used to set the local heat flux on the vessel outer wall (A).

- **Conducting Walls**: the IHX shell (B) is actually meshed and conjugate heat transfer is calculated on these solid cells.

- **Fixed temperature walls**: heat fluxes through the walls listed below are simulated by setting a fixed temperature with a given resistance corresponding to the wall characteristics (conductivity and width):

  – Tube walls: fixed temperature at $400\ ^oC$ with resistance $r = 5.5{\cdot}10^{-5}\ m^2\,K\,W^{-1}$.

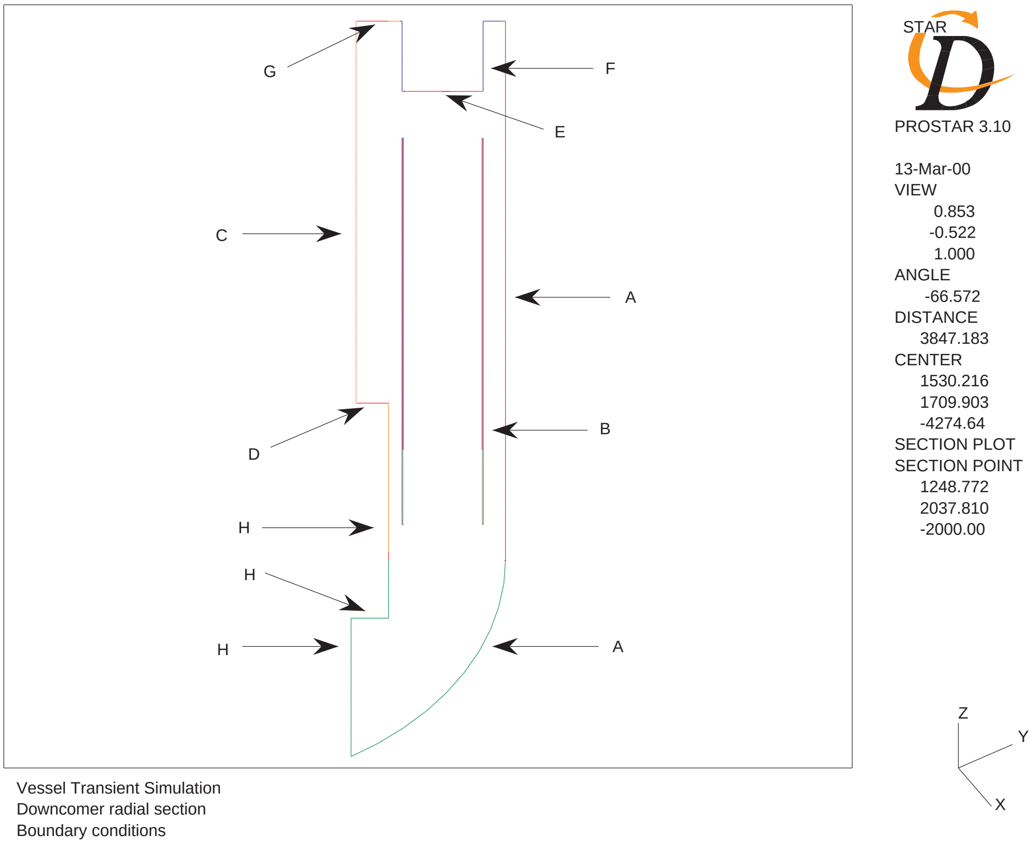

Figure 2: Solid walls of the downcomer channel: (A) outer wall, (B) IHX shell, (C) inner wall behind the tubes, (D) rising tubes support, (E) bottom of IHX feeding tube connection, (F) lateral of IHX feeding tube connection, (G) cover wall, (H) inner walls under the pipes.

Material	Pb-Bi	oil	solid	Total
Number of cells	142,318	29,040	11,200	182,558

Table 1: Number of cells used for the numerical simulation for each material and for the whole domain.

$\Delta P_f(Pa)$	$\Delta P_b(Pa)$	$\xi(adim)$
3342	3488	11.8

Table 2: Pressure loss by friction in the IHX (ΔP_f) and buoyant pressure (ΔP_b) with the friction factor ξ.

  - Wall behind the tubes (C): fixed temperature at $400\ ^oC$ with resistance $r = 2. \cdot 10^{-3}\ m^2\, K\, W^{-1}$.
  - Rising tubes support (D): fixed temperature at $400\ ^oC$ with resistance $r = 1. \cdot 10^{-3}\ m^2\, K\, W^{-1}$.
  - Bottom of IHX feeding tube connection (E): fixed temperature at $320\ ^oC$ with resistance $r = 6. \cdot 10^{-3}\ m^2\, K\, W^{-1}$.
  - Lateral and top of IHX feeding tube connection (F): fixed temperature at $320\ ^oC$ with resistance $r = 1.5 \cdot 10^{-3}\ m^2\, K\, W^{-1}$.

- **Adiabatic Walls** The cover wall (G) and the inner walls under the pipes (H), separating the downcomer from the core region, are treated as adiabatic.

5.7 Mesh structure

The domain has been meshed following a block-structured strategy. The first $6.92\ m$ ($4.5\ m$ for the inlet tubes) are constructed by extruding the planar 2D-mesh shown in figure 3 while the bottom part is just one structured 3D-block. The connection to the upper part is non-matching. The number of cells used for the numerical simulation for each material and for the whole domain is shown in table 1.

6 Results

The simulation is pseudo-transient using 1200 iterations of 0.05s of the SIMPLE algorithm. It is a restart simulation a converged simulation at nominal power.

The pressure loss ΔP_f calculated from the numerical integration of the losses inside the IHX (equation 16) and the buyancy pumping pressure, ΔP_b, as calculated by equation 19, are reported in table 2 for the normal operation condition. We give

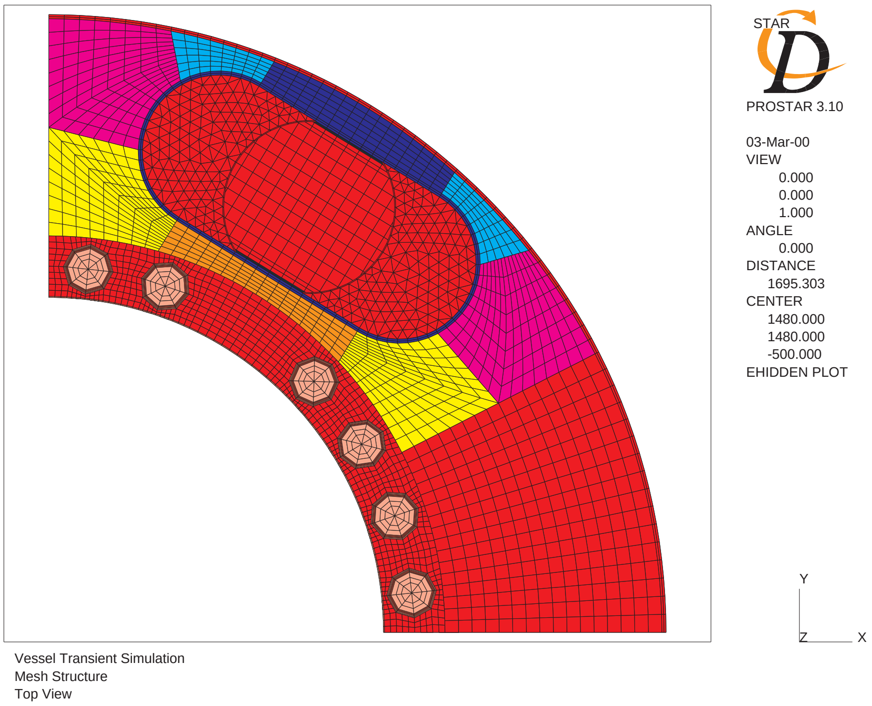

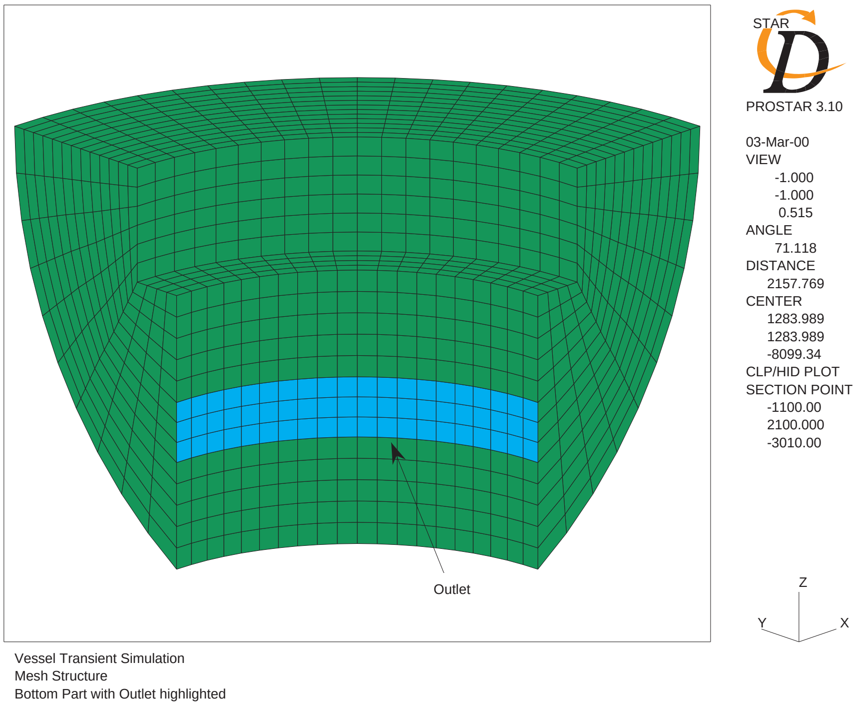

Figure 3: One quarter of the EADF. Mesh structure of an horizontal section and bottom mesh with outlet localization.

Mass flow rate (kg/s)	Inside IHX	Outside IHX	bypass fraction
initial time	1418.0	31.7	2.19 %
10s	1404.3	63.8	4.35 %
20s	1368.0	97.7	6.67 %
30s	1322.7	144.9	9.87 %
40s	1301.7	173.1	11.74 %
50s	1266.5	201.7	13.73 %
60s	1228.9	239.2	16.29 %

Table 3: Mass flow rate inside and bypassing the IHX every $10s$.

Time (s)	Heat power absorbed by the IHX (kW/s)	Heat power exchanged by the oil columns (kW/s)
0	20,750	3,931
10	20,616	3,926
15	20,061	3,889
20	19,147	3,796
25	17,747	3,632
30	16,603	3,413
40	15,533	3,065
50	14,577	2,809
60	13,499	2,582

Table 4: Heat exchanges inside the IHX at different times.

also ξ, the corresponding friction factor, calculated with equation 20. All these numbers refer to the initial conditions.

We plot the mean temperature profiles along the vertical axis every $10\ s$ for the first sixty seconds in Figures 4 to 7. These values are calculated by averaging on each plane of cells and taking separately into account all fluid cells which are inside and outside the IHX. All fluid cells located under the IHX are considered inside the IHX.

The thermal stratification plays an important role in the fatigue analysis. In figures 8 and 9, we shows an history of the temperature distribution of the primary coolant through the downcomer channel. In figures 10 and 11, we show the same history of the temperature field of the primary coolant close to the inner walls and to the outer wall of the downcomer channel.

The mass flow rates inside and bypassing the IHX are given in table 3.

The heat exchanges inside the IHX are given in table 4. It can be seen that while the mass flow rate diminution is about 15 %, the loss of power is about 33 %. In effect, the power loss is due both to the diminution of the mass flow rate and to the diminution of the temperature in the IHX inlet.

In figure 12, we present the monitored cell value history curves. The monitored cell is taken at the center of the IHX, giving an idea of the mass flow rate evolution and of the temperature evolution inside the IHX. It can be seen that the change in temperature is noticeable only after 400 iterations (that is $20\,s$).

7 Conclusion

We have performed a 3D transient simulation of the EADF downcomer channel coupled with the IHX taking into account all relevant heat transfer phenomena. The simulation represents the first $60\,s$ of a the core reactor shutdown operation with constant volume flow rate. One minute is not enough to reach a new stationary flow configuration. The IHX operation conditions start changing after $20\,s$ from the beginning of the simulation. The incoming cold flow starts renewing the hot fluid region with a progressive increase of the by-pass flow rate.

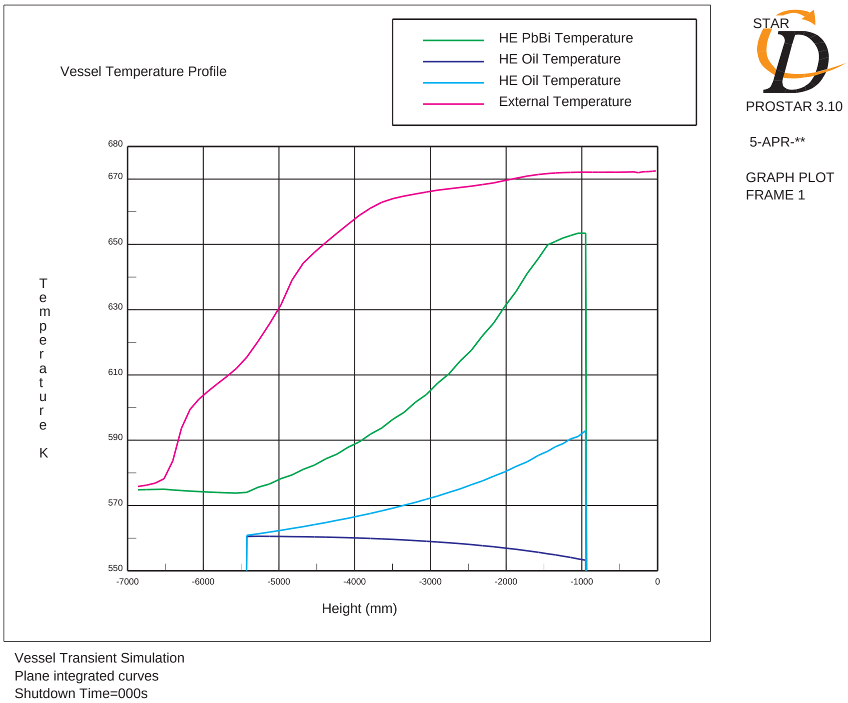

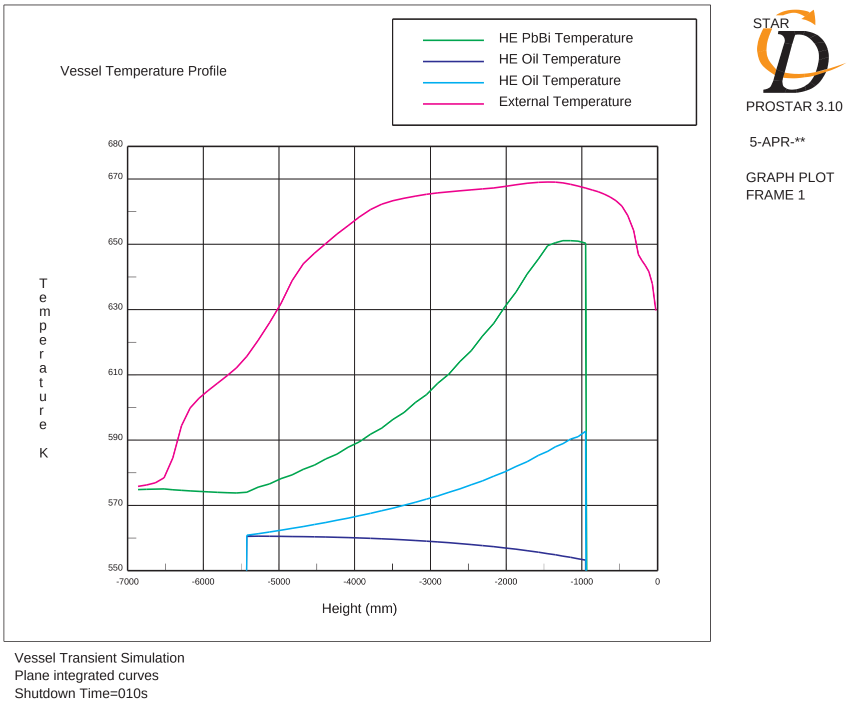

Figure 4: Mean temperature profiles along the vertical axis at initial time (upper) and after $10\,s$ (lower).

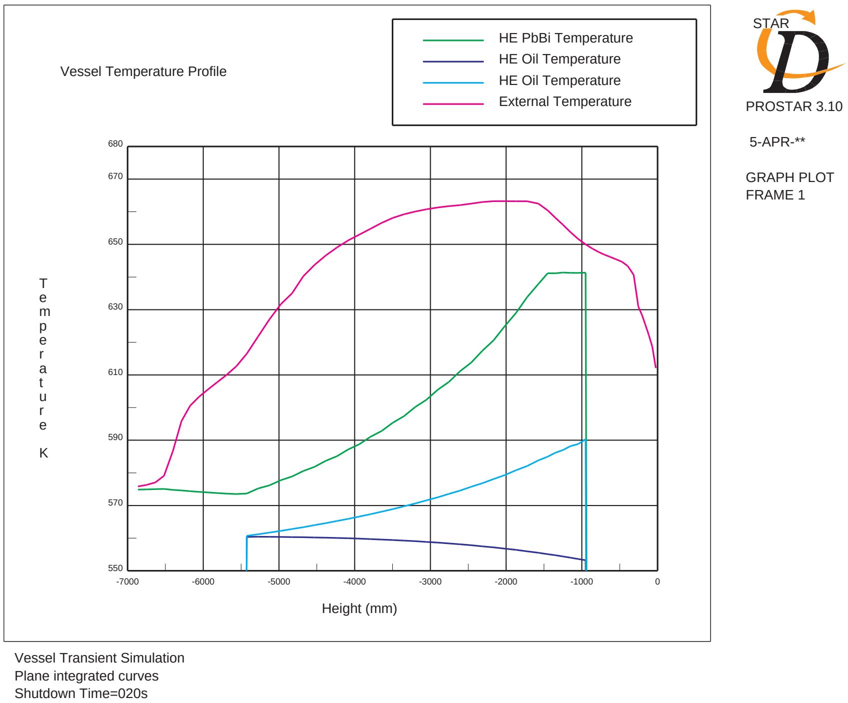

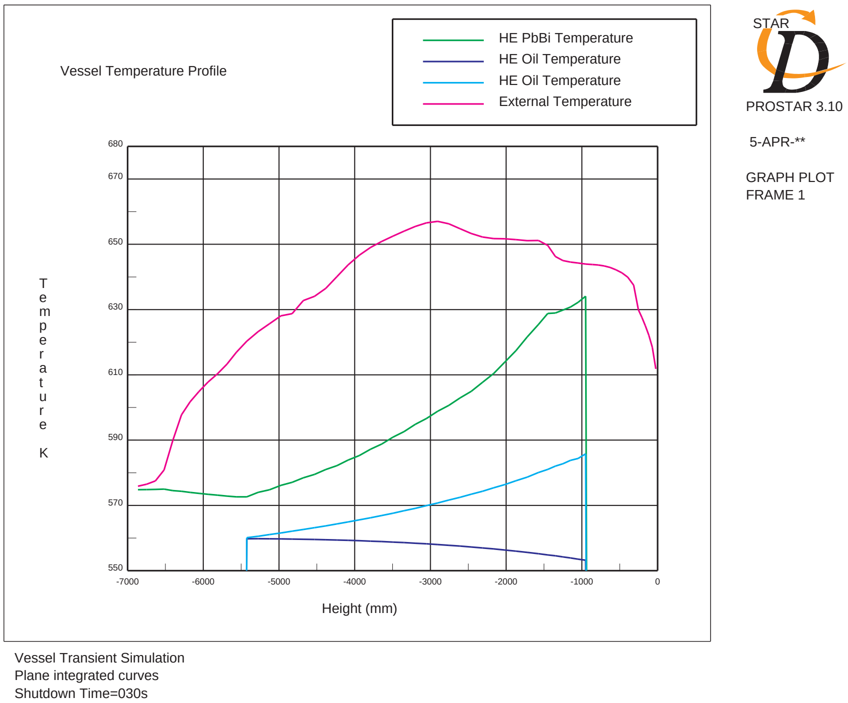

Figure 5: Mean temperature profiles along the vertical axis after $20\,s$ (upper) and $30\,s$ (lower).

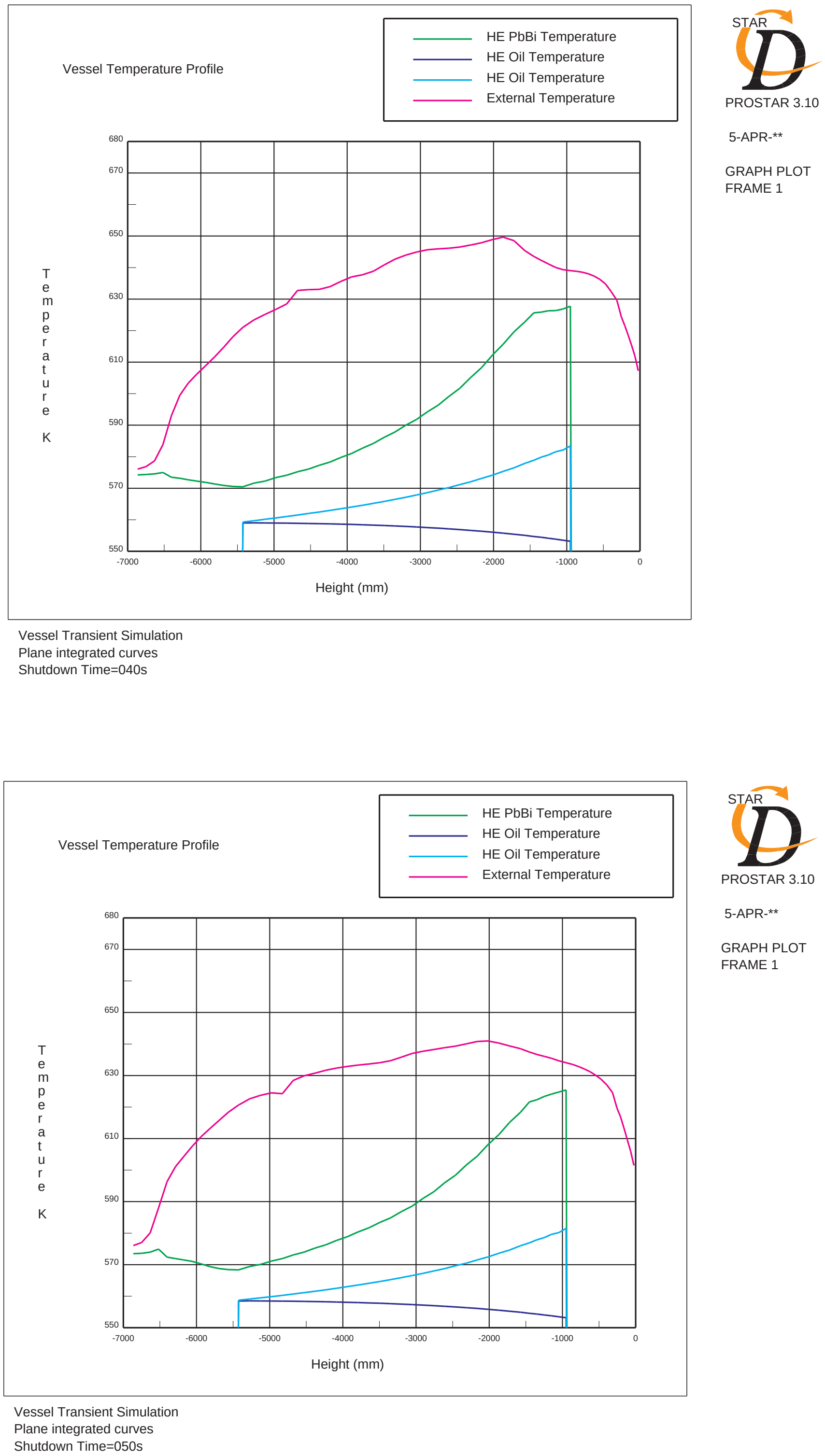

Figure 6: Mean temperature profiles along the vertical axis after $40\,s$ (upper) and $50\,s$ (lower).

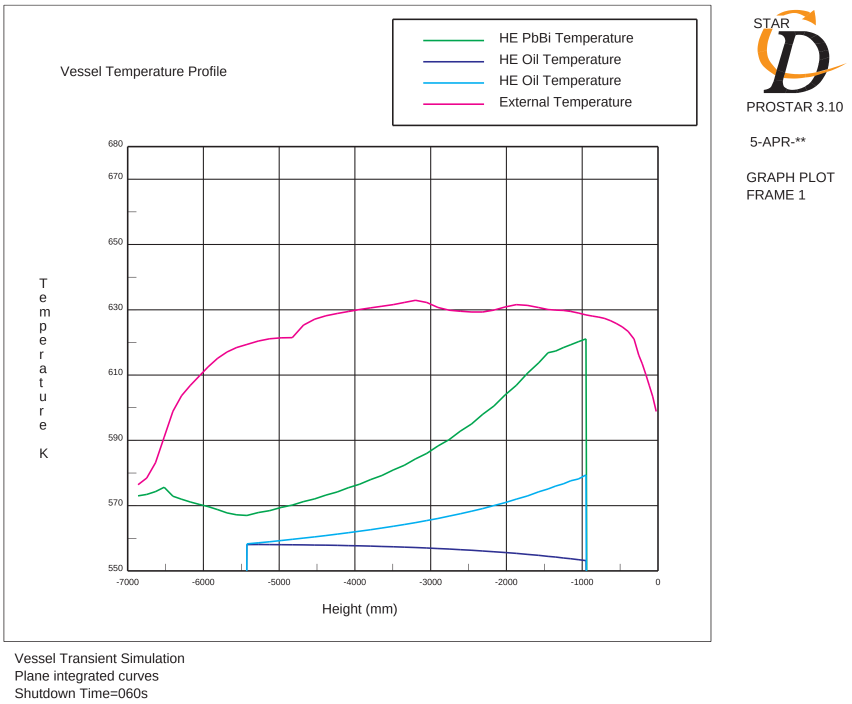

Figure 7: Mean temperature profiles along the vertical axis after $60\,s$.

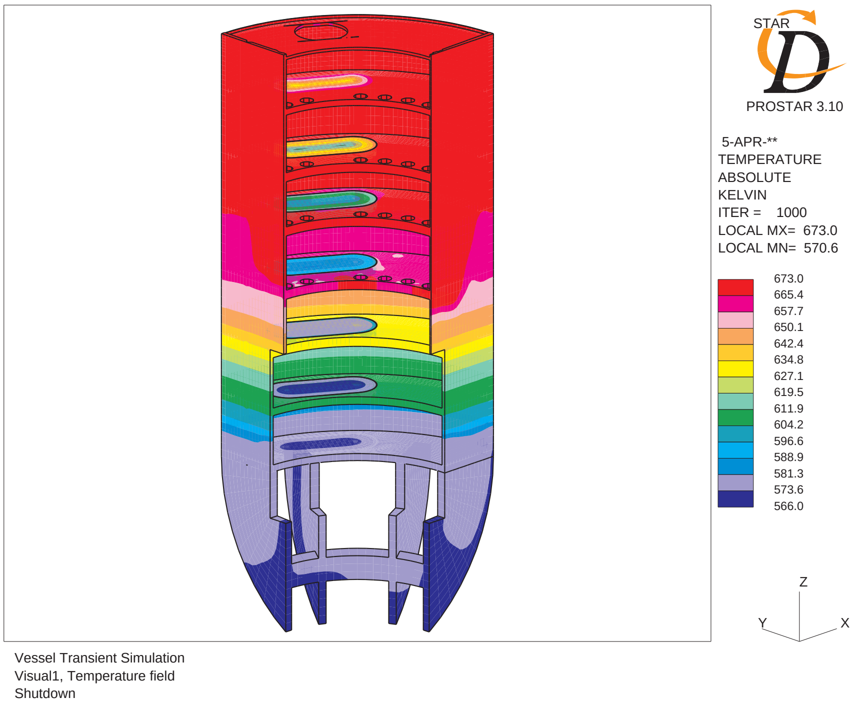

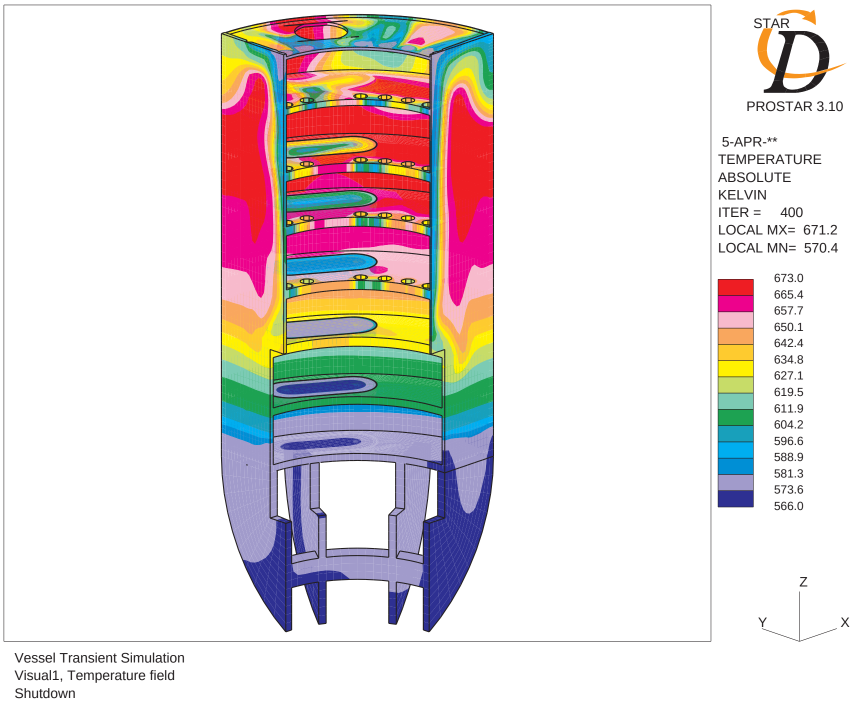

Figure 8: Temperature distribution of the primary coolant throughout the downcomer channel at time $t = 0\,s$ and $t = 20\,s$.

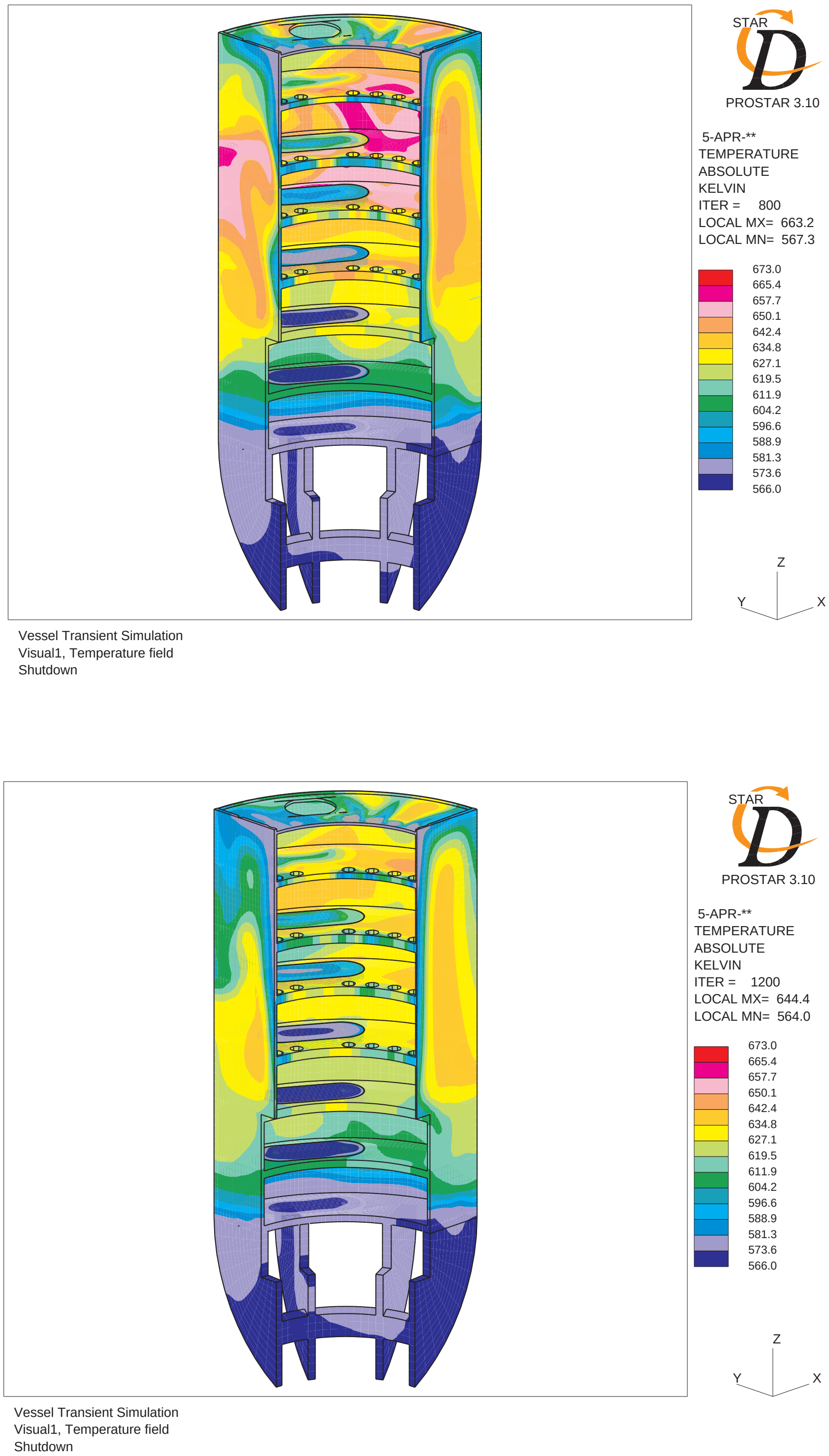

Figure 9: Temperature distribution of the primary coolant throughout the downcomer channel at time $t = 40\,s$ and $t = 60\,s$.

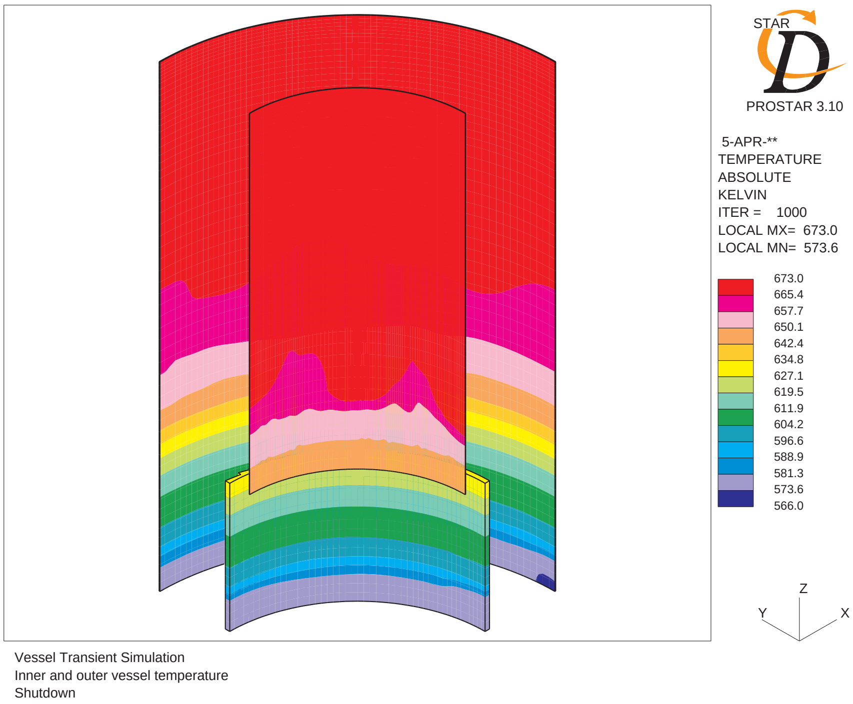

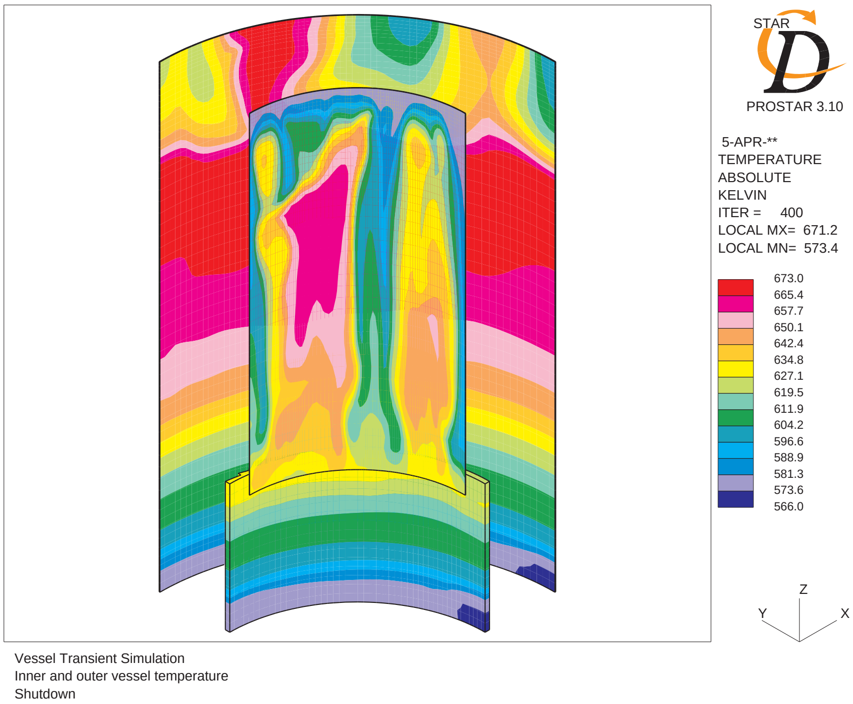

Figure 10: Temperature distribution of the primary coolant along the inner and outer wall of the downcomer channel at time $t = 0\,s$ and $t = 20\,s$.

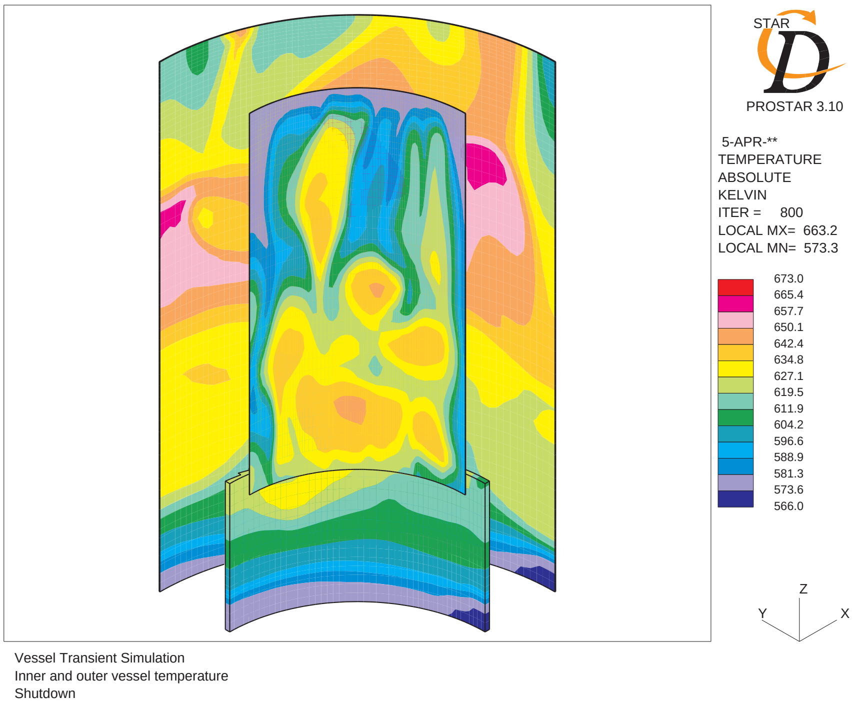

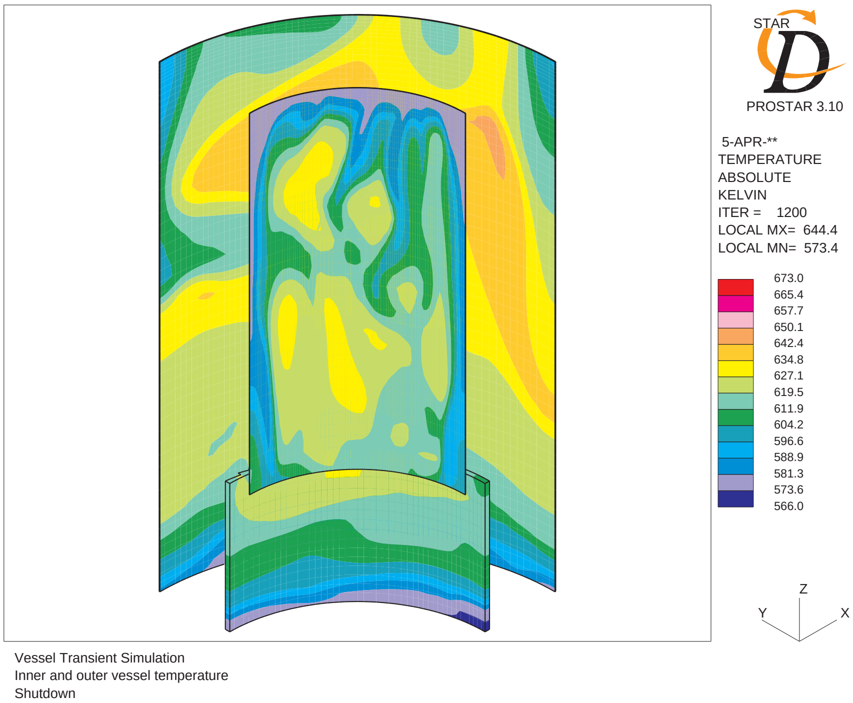

Figure 11: Temperature distribution of the primary coolant along the inner and outer wall of the downcomer channel at time $t = 40\,s$ and $t = 60\,s$.

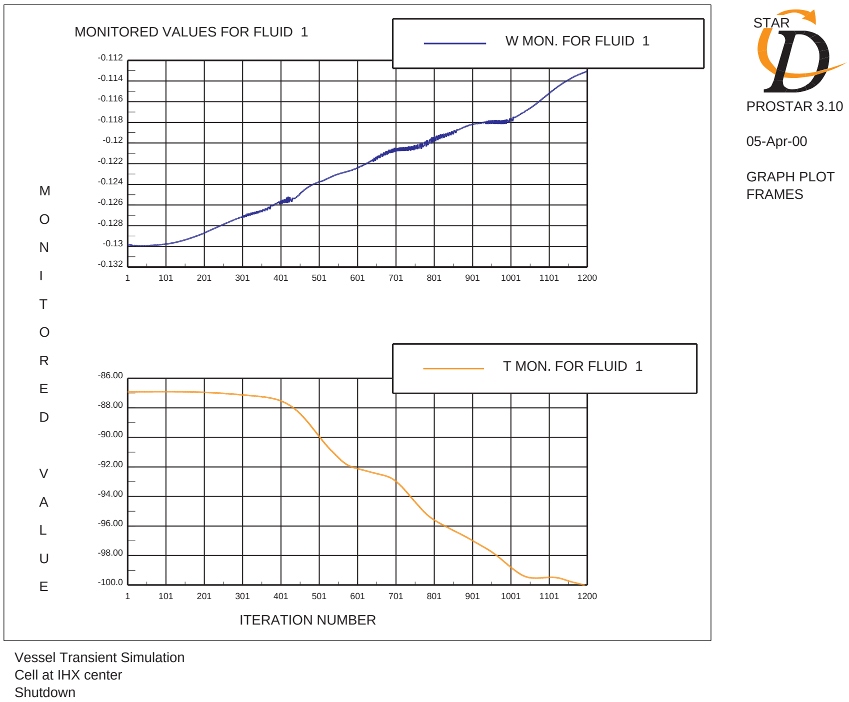

Figure 12: Monitored value at IHX center. The temperature curve is relative to the reference temperature $T_{ref} = 400\,^{o}C$.

References

[1] C. Rubbia et al. Conceptual design of a fast neutron operated high power energy amplifier. Technical Report CERN/AT/95-44(ET), CERN, Geneva, September 29 1995.

[2] Ansaldo; CRS4; ENEA; INFN. Energy amplifier demonstration facility reference configuration. summary report. Technical Report Ansaldo Report EA B0.00 1 200, Ansaldo, Genova, January 1999.

[3] G. Bianchini; M. Carta; A. D'Angelo; F. Norelli. New mathematical models implemented in tieste-minosse code. Technical report, ENEA Divisione Sistemi Energetici Ecosostenibili, 02 2000. DT-SDA-00023.

[4] Corsini. Primary coolant temperature profiles in the downcomer of the adsdf. Technical Report ADS 5 TRLX 0275, ANSALDO, 1999.

[5] L. Maciocco; V. Bellucci; S. Buono; G. Fotia; V. Moreau; M. Mulas; G. Siddi; L. Sorrentino. Design and optimisation of a liquid metal spallation target for the energy amplifier prototype. In *AccApp'98 2nd International Topical Meeting on Nuclear Applications of Accelerator Technology*, La Grange Park Illinois 60526 USA, Septembre 20-23 1998. American Nuclear Society Inc.

[6] V. Bellucci; S. Buono; G. Fotia; L. Maciocco; V. Moreau; M. Mulas; G. Siddi; L. Sorrentino. Thermalhydraulic design of the fuel element of the energy amplifier prototype. Technical report, CRS4, 1998.

[7] V. Bellucci; S. Buono; L. Maciocco; V. Moreau; L. Sorrentino. Numerical simulation of the energy amplifier demonstration facility vessel. Technical report, CRS4, 1999. Internal Note 99-2.

[8] L. Sorrentino C. Aragonese; S. Buono; G. Fotia; L. Maciocco; V. Moreau. A thermal fluid-dynamic steady state analysis of the eadf downcomer channel. TECH-REP 00/07, CRS4, 2000.

[9] S. Buono. Minutes of the first meeting of the benchmark working group on heavy liquid metal thermal-hydraulics. CERN Geneva, June 29-30 1999.

[10] Jaffrelot Michel. Dimensionnement et optimisation de l'échangeur de chaleur du prototype de l'amplificateur d'energie. Master's thesis, Ecole des mines d'Albi, 1998.

[11] Computational Dynamics Limited. *Methodology STAR-CD version 3.10*, 1999.

[12] C. Aragonese; S. Buono; L. Maciocco; V. Moreau; L. Sorrentino. A heat exchanger design for the separated window target of the eadf. Technical report, CRS4, 2000. to appear.

[13] Ansaldo. Personal communication.